Hindawi
Shock and Vibration
Volume 2021, Article ID 5537622, 9 pages
https://doi.org/10.1155/2021/5537622

Research Article

Wind-Induced Vibration Control of High-Rise Structures Using Compound Damping Cables

Jianda Yu,[1,2] Zhibo Duan,[1] Xiangqi Zhang,[1] and Jian Peng[1,2]

[1]*School of Civil Engineering, Hunan University of Science and Technology, Xiangtan 411201, Hunan, China*
[2]*Hunan Provincial Key Laboratory of Structures for Wind Resistance and Vibration Control, Hunan University of Science and Technology, Xiangtan 411201, Hunan, China*

Correspondence should be addressed to Jian Peng; pengjian@hnu.edu.cn

Received 1 February 2021; Revised 2 April 2021; Accepted 13 April 2021; Published 22 April 2021

Academic Editor: Yaobing Zhao

Based on the vibration reduction mechanism of compound damping cables, this study focuses on the wind-induced vibration control of high-rise structures with additional mass at the top. The differential equation of motion of the system under the action of the composite damping cable is established, and the analytical solution of the additional damping ratio of the structure is deduced, which is verified by model tests. The vibration response of the structure under the action of simple harmonic vortex excitation and randomly fluctuating wind loads is studied, and the effect of different viscous coefficients of the dampers in the composite damping cable and different installation heights of the damping cable on the vibration control is analyzed. The results show that a small vortex excitation force will cause large vibrations of low-dampened towering structures, and the structure will undergo buffeting under the action of wind load pulse force. The damping cable can greatly reduce the amplitude of structural vibration. The root means square of structural vibration displacement varies with damping. The viscosity coefficient of the device and the installation height of the main cable of the damping cable are greatly reduced.

1. Introduction

With the development of the social economy and technological progress, various towering structures have emerged constantly. High-rise structures often have the characteristics of a large slenderness ratio and or low damping. Under the action of earthquake and wind load, large vibrations are prone to cause fatigue cracks and even collapse. In addition, some towering structures have huge additional mass at the top, which reduces the natural frequency of the structure, increases the wind load the structure bears, and makes the wind-induced vibration of the structure more significant. For example, steel structure high-pier rigid frame bridges in the construction stage are prone to buffeting or vortex-induced resonance due to wind loads [1, 2]. The wind turbine tower with a height of more than 120 m has low rigidity and low damping. The nacelle and blades on the top of the tower not only increase the mass but also greatly increase the wind load on the tower; then, the wind turbines are prone to large vibrations under wind load [3–5]. Therefore, it is important to investigate the vibration control problem of the high-rise structure.

For large-scale vibration control of high-rise structures, additional damping devices are mainly used for vibration control. Battista et al. [6] studied the dynamic behavior and stability of transmission line tower under wind forces and the vibration control of the tower using the nonlinear pendulum-like dampers. Zhang et al. [7] investigated the seismic control of power transmission tower using pounding tuned mass dampers (TMD). Carrato et al. [8] investigated the tuned mass damper control of cross-wind excitation of a solar tower. Xiang et al. [9] studied seismic vibration control of building structures with multiple tuned mass dampers. Peng et al. [10] studied the large-scale vibration control of a long-span cable-stayed beam under time-delay technology. Zhou et al. [11] investigated the optimum problem on wind-induced vibration control of high-rise buildings with viscous dampers. Li et al. [12, 13] studied the effects of structural damping on wind-induced responses of a 243 m high solar tower based on a novel elastic test model and mitigation of

wind-induced responses of a cylinder solar tower by a tiny eddy current tuned mass damper based on elastic wind tunnel tests. Wang et al. [14] investigated the wind-induced response control of high-rise buildings using inerter-based vibration absorbers. Wang et al. [15] studied the wind-induced vibration control and parametric optimization of connected high-rise buildings with tuned liquid column damper-inerter.

In general, these studies used different additional dampers to control the vibration of the high-rise structure and achieved better suppression effects. In particular, tuned mass dampers (TMD) are used for vibration reduction. When the structure vibration frequency is high, TMD has a better suppression effect on the structure, but each TMD can only suppress the vibration of one frequency of the structure, which is suitable for the towering and flexible The vibration suppression effect of the structure with multiple frequencies or varying frequencies is poor. Moreover, the multimodal and ultra-low frequency vibration of the existing high-rise structures puts forward higher requirements for vibration reduction, and there is an urgent need for an efficient and economical vibration reduction method.

Therefore, in this study, a vibration reduction method of compound damping cables is presented [16], and then, the wind-induced vibration control of high-rise structures using compound damping cables are investigated. Taking the flexible column installed by an additional mass on the top as the research object, the Lagrangian equation is used to establish the composite damping cable-tall structure vibration differential equation, and the analytical solution of the additional damping ratio is obtained. Model tests are used to verify the accuracy of the analytical solution. Then, the damping effect of damping cables on wind-induced buffeting and vortex-induced resonance of high-rise structures is analyzed. Then, we organize the rest of this study as follows. In Section 2, we introduce the mechanical model of high-rise structures with compound damping cable. In sections 3 and 4, the characteristic problem and experimental verification are discussed, respectively. Then, the wind-induced vibration response is investigated in Section 5. A summary of results is presented in Section 6.

2. Mechanical Model

As shown in Figure 1(a), compound damping cable includes main cable, auxiliary cable, hanger, spring, damper, and return spring. The main cable can be approximated to a straight line under a small tension due to the pulling force of n booms with a reasonable spacing. A return spring with a smaller stiffness and a damper are connected in series on the main cable. When a high-rise structure undergoes lateral bending vibration, since the tension stiffness of the main cable is much greater than that of the return spring, the deformation of the main cable is small, and the two ends of the return spring have a relatively large relative displacement. Dampers consume a lot of energy and can quickly reduce the mechanical energy of high-rise structures, which is driven by the large relative movement of the two ends of the return spring.

2.1. Stiffness of the Primary Cable. For stay cables, as shown in Figure 1(b), the cable sag is large due to the action of gravity load, which reduces the tensile stiffness of the cable and becomes more obvious with the increase of the span of the cable.

According to Ernst's formula [17], the tensile equivalent elastic modulus of the cable is obtained as

$$E_{eq} = \frac{E_e}{1 + \left(\gamma^2 L^2 / 12\sigma^3\right) E_e} = \mu E_e, \tag{1}$$

where E_e is the elastic modulus of the cable material, γ is the gravity per unit volume of the cable, L is the span of the cable, and σ is the axial normal stress of the cable. For long-span cable, if σ remains the same, with the increase of span L, a reduction factor of elastic modulus μ is approximately inversely proportional to quadratic cable span L. By applying a transverse force F in the middle span, the cable sag can be reduced as f_2 as shown in Figure 1(b). Under the condition of the same cable force, the factor μ will increase significantly. If n transverse external forces are applied at equal intervals of the stay cable to decrease the sag of the cable, μ will increase with the increase of n until it approaches one, as shown in Figure 1(a).

The role of the secondary cable and the hanger is only to ensure that the main cable is easier to be straightened, and the energy consumption effect of the secondary cable can be ignored. The simplified mechanical model of the composite damping cable is shown in Figure 1(c). The main parameters include the mass per unit length of a homogeneous column with uniform cross-section is m_ρ, the additional mass at the top of the column is M, the column bending stiffness is EI, the return spring stiffness is k_2, the main cable stiffness is k_3, the damper mass is m_d, and the viscosity coefficient is c. The main cable of the composite damping cable is installed between section B of the structural column and the ground. The height of the main cable is h, the inclination angle is θ, the pretension is F_N, and the column height is H.

2.2. Equation of Motion. The motion equation of the high-rise flexible structure with compound damping cable can be obtained by using Lagrange's equation, which can be expressed as

$$\frac{\mathrm{d}}{\mathrm{d}t}\left(\frac{\partial T}{\partial \dot{q}_j}\right) - \frac{\partial T}{\partial q_j} + \frac{\partial U}{\partial q_j} + \frac{\partial \Psi}{\partial \dot{q}_j} = Q_j(t), \quad j = 1, 2, \ldots, n_1, \tag{2}$$

where q_j and $\dot{q}_j$ are the generalized coordinates and generalized velocity of the system, respectively, T is the kinetic energy, U is the potential energy, Ψ is the dissipated energy, $Q_j(t)$ is the external excitation corresponding to the generalized coordinate q_j, and n_1 is the number of degrees of freedom of system. The expression is as follows:

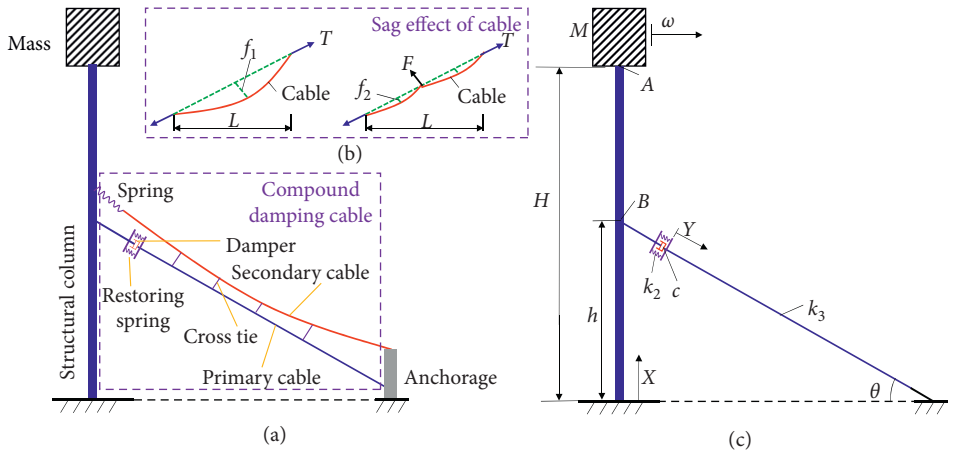

FIGURE 1: The simple controlled beam structure model.

$$T = \frac{1}{2}m_\rho \int_0^H \dot{v}(x,t)^2 \mathrm{d}x + \frac{1}{2}M\dot{v}(x_A,t)^2 + \frac{1}{2}m_d\dot{y}^2, \tag{3}$$

$$U = \frac{1}{2}EI\int_0^H \left(\frac{\partial^2 v(x,t)}{\partial x^2}\right)^2 \mathrm{d}x + \frac{1}{2}k_2\left(v(x_B,t)\cos\theta - y\right)^2 + \frac{1}{2}k_3y^2, \tag{4}$$

$$\Psi = \frac{1}{2}c\left(\frac{\partial v(x_B,t)}{\partial t}\cos\theta - \dot{y}\right)^2, \tag{5}$$

where $v(x,t)$ is the vibration displacement function of the column, $v(x,t) = Z(t)\phi(x)$, $Z(t)$ is the vibration function of any section of the column, and $\phi(x)$ is the mode shape of the column. For the first-order mode, the expression of the mode shape is as follows:

$$\phi(x) = \cosh\left(\frac{\omega_1 x}{H}\right) - \cos\left(\frac{\omega_1 x}{H}\right) - \frac{\cosh(\omega_1)+\cos(\omega_1)}{\sinh(\omega_1)-\sin(\omega_1)}\left(\sinh\left(\frac{\omega_1 x}{H}\right) - \sin\left(\frac{\omega_1 x}{H}\right)\right), \tag{6}$$

where ω_1 is the first-order frequency, x is the position of the section, and H is the height of the column, as shown in Figure 1.

Substituting equations (3)–(5) into equation (2), we can obtain the vibration control equation of the high-rise flexible structure with compound damping cable:

$$\begin{aligned} &m_\rho\ddot{Z}(t)\int_0^H \phi^2(x)\mathrm{d}x + M\ddot{Z}(t)\phi^2(x_A) + EIZ(t)\int_0^H \left(\frac{\mathrm{d}^2\phi(x)}{\mathrm{d}x^2}\right)^2 \mathrm{d}x + k_2\left(\phi(x_B)Z(t)\cos\theta - y\right)\phi(x_B)\cos\theta \\ &\quad = -c\left(\dot{Z}(t)\phi(x_B)\cos\theta - \dot{y}\right)\phi(x_B)\cos\theta, \end{aligned} \tag{7a}$$

$$m_d\ddot{y} - k_2\left(\phi(x_B)Z(t)\cos\theta - y\right) + k_3y = c\left(\dot{Z}(t)\phi(x_B)\cos\theta - \dot{y}\right). \tag{7b}$$

3. Characteristic Problem

To better understand the response of the system, so in this section, the characteristic problem are studied. Since $m_d \ll M$, ignoring the influence of the damper's inertial force, equations (7a) and (7b) can be written as

$$\begin{aligned}\ddot{Z}\left[c\left(m_\rho\int_0^H\phi^2(x)\mathrm{d}x+M\phi^2(x_A)\right)\right]+\ddot{Z}(t)\left[(k_2+k_3)\left(m_\rho\int_0^H\phi^2(x)\mathrm{d}x+M\phi^2(x_A)\right)\right]\\+\dot{Z}(t)\left[ck_3\phi^2(x_B)\cos^2\theta+cEI\int_0^H\left[\frac{\mathrm{d}^2\phi(x)}{\mathrm{d}x^2}\right]^2\mathrm{d}x\right]\\+Z(t)\left[k_2k_3\phi^2(x_B)\cos^2\theta+(k_2+k_3)EI\int_0^H\left[\frac{\mathrm{d}^2\phi(x)}{\mathrm{d}x^2}\right]^2\mathrm{d}x\right]=0.\end{aligned}\tag{8}$$

Then, the characteristic equation of equation (8) is as follows:

$$a_1s^3+b_1s^2+c_1s+d_1=0,\tag{9}$$

where

$$\begin{aligned}a_1&=c\left(m_\rho\int_0^H\phi^2(x)\mathrm{d}x+M\phi^2(x_A)\right),\\b_1&=(k_2+k_3)\left(m_\rho\int_0^H\phi^2(x)\mathrm{d}x+M\phi^2(x_A)\right),\\c_1&=ck_3\phi^2(x_B)\cos^2\theta+cEI\int_0^H\left[\frac{\mathrm{d}^2\phi(x)}{\mathrm{d}x^2}\right]^2\mathrm{d}x,\\d_1&=k_2k_3\phi^2(x_B)\cos^2\theta+(k_2+k_3)EI\int_0^H\left[\frac{\mathrm{d}^2\phi(x)}{\mathrm{d}x^2}\right]^2\mathrm{d}x.\end{aligned}\tag{10}$$

When the viscosity coefficient of the damper $c = 0$, the natural frequency of the structure can be obtained.

$$\omega_n=\sqrt{\frac{d_1}{b_1}}.\tag{11}$$

Then, we introduce

$$\begin{aligned}A&=b_1^2-3a_1c_1,\\B&=b_1c_1-9a_1d_1,\\C&=c_1^2-3b_1d_1.\end{aligned}\tag{12}$$

When $\Delta = B^2 - 4AC = 0$, the three roots s_1, s_2, and s_3 of equation (9) can be written as

$$s_1=\frac{-b_1-\left(\sqrt{[3]}\,\Upsilon_1+\sqrt{[3]}\,\Upsilon_2\right)}{3a_1},\tag{13}$$

$$s_{2,3}=\frac{-b_1+(1/2)\left(\sqrt{[3]}\,\Upsilon_1+\sqrt{[3]}\,\Upsilon_2\right)\pm(\sqrt{3}/2)\left(\sqrt{[3]}\,\Upsilon_1-\sqrt{[3]}\,\Upsilon_2\right)i}{3a_1},\tag{14}$$

where $Y_{1,2}=Ab_1+3a_1(-B\pm\sqrt{B^2-4AC}/2), i^2=-1$. Therefore, the general solution of equation (8) can be obtained:

$$z(t)=\chi_1e^{s_1t}+e^{s_4t}\left(\chi_2e^{is_5t}+\chi_3e^{-is_5t}\right),\tag{15}$$

where

$$\begin{aligned}s_4&=\frac{-b_1+(1/2)\left(\sqrt{[3]}\,\Upsilon_1+\sqrt{[3]}\,\Upsilon_2\right)}{3a_1},\\s_5&=\frac{(\sqrt{3}/2)\left(\sqrt{[3]}\,\Upsilon_1-\sqrt{[3]}\,\Upsilon_2\right)}{3a_1}.\end{aligned}\tag{16}$$

The first term in equation (13) decays rapidly during structural vibration, which is a real solution. Therefore, free

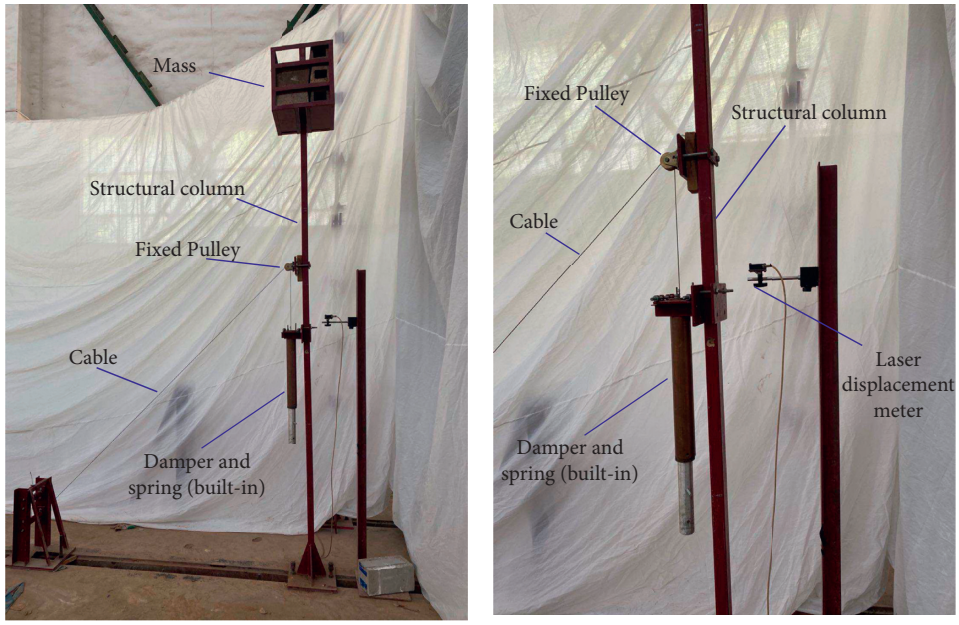

(a) (b)

Figure 2: Experiment site photos of high-rise structure and composite damper cable.

vibration is only related to the complex solutions of the second and third terms. The damping ratio of the system is

$$\zeta = -\frac{s_4}{\omega_n} = -\frac{-b_1 + (1/2)\left(\sqrt{[3]}\,\Upsilon_1 + \sqrt{[3]}\,\Upsilon_2\right)}{3a_1\omega_n}. \tag{17}$$

For a low-damping system, when the assumed mode shape is consistent with the actual mode shape of the structure, equation (13) can obtain an accurate solution for the compound damping cable to provide additional damping ratio for the structure. When only a small error exists between the assumed mode and the actual mode of the structure, the approximate solution of the additional damping ratio provided by the composite damping cable for the structure can be approximately obtained from equation (14). For the column structure, its mode shape is approximately obtained as

$$\varphi(x) = \frac{3Hx^2 - x^3}{6H^3}, \quad 0 \le x \le H. \tag{18}$$

4. Experimental Verification

4.1. Experimental Model. In order to verify the correctness of the theoretical analysis results, the model test of the damping cable-column structure is first carried out. The height of the column model is 3 m, and the cross-section is a rectangular steel tube with a cross-section of 60 mm × 40 mm × 3.5 mm. The lower end of the column is anchored, and the upper end is free. For the small sag main cable of the model test, the role of the secondary cable is not required, so the damping cable only contains the main cable, the return spring, and the eddy current damper, and the main cable diameter is 1.5 mm steel wire rope. The photo of the test site is shown in Figure 2, and the parameter values are given in Table 1. Experiment parameters are as follows: $H = 3.0$ m, $h = 2.0$ m, $M = 160$ kg, $m_d = 0.6$ kg, $\theta = \pi/4$, $k_2 = 3368$ N/m, $k_3 = 22384$ N/m, and $F_N = 100$ N. The eddy current damper is composed of a copper tube and a magnet. The relationship between the number of magnets and the viscous damping coefficient of the eddy current damper is given in Table 1.

4.2. Comparative Analysis. The artificial excitation method is used to make the structure vibrate. When the structure amplitude reaches the set value, the excitation is suddenly removed, and the structure continues to vibrate freely. Use the SYNERGY data acquisition system to collect data on structural vibration displacement, and the damping ratio is calculated by the envelope method.

$$x = Ae^{-\zeta\omega_n t}\sin(\omega_d t), \tag{19}$$

where A is the initial amplitude of free vibration, ζ is the equivalent damping ratio, ω_n is the natural frequency of the structure, and $\omega_d = \omega_n\sqrt{1-\zeta^2}$.

Figure 3 shows the vibration displacement time history curve of the structure. When the composite damping cable is not installed, the damping ratio of the structure itself is 0.16%. When installing compound damping cables on the structure, change the number and thickness of magnets in the eddy current damper and measure the typical displacement time history curve of structural vibration. When $c = 0$ shows the displacement attenuation time history when the damping cable is not installed with a damper. The cable pretension acts on the fixed pulley, and the friction of the fixed pulley can consume part of the energy of structural vibration. $c = 72$ Ns/m and $c = 236$ Ns/m show that the displacement attenuation time history of the damping cable

Table 1: Viscous damping coefficient of eddy current damper.

Number of magnets	1	2	3	4	5	6
Viscous damping coefficient (Ns/m)	28	72	113	153	195	236

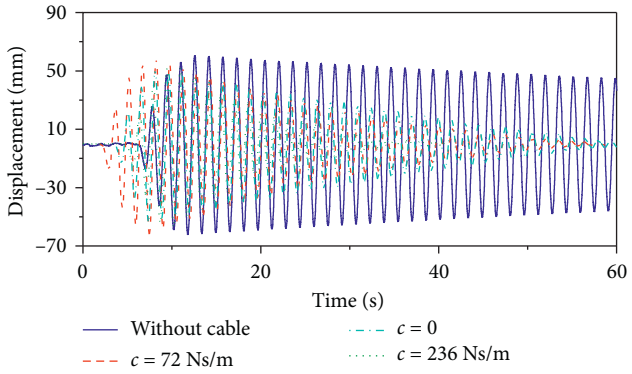

Figure 3: The time history curve of the system with different damping coefficients c.

when eddy current dampers with different damping coefficients is installed. It can be seen from the figure that the damping cable can efficiently consume the energy of structural vibration, so that the vibration of the structure is attenuated quickly.

According to equation (15), the equivalent damping ratio of the structure under each viscous damping coefficient can be obtained. The experimental values of the additional damping ratio of the eddy current damper under different viscous coefficients are given in Table 2.

The additional damping ratio test value ζ^E includes two parts: the sum of the damping ratio of the pulley friction caused by the main cable pretension and the damping ratio of the structure itself ζ_f^E and the damping ratio of the viscous damper ζ_c^E.

$$\zeta^E = \zeta_f^E + \zeta_c^E, \tag{20}$$

Table 2: Additional damping ratio experimental value of high-rise structure.

c (Ns/m)	0	28	72	113	153	195	236
ζ^E (%)	0.67	0.88	1.13	1.50	1.82	2.03	2.29
ζ_c^E (%)	0	0.21	0.47	0.84	1.15	1.36	1.62
ζ^T (%)	0	0.19	0.48	0.76	1.03	1.31	1.59

where ζ_f^E is the damping ratio measured in the experiment when the viscous coefficient of the damper $c = 0$. The relationship between the measured viscous damper damping ratio ζ_c^E and the damping ratio ζ^T is shown in Figure 4.

It can be seen from Figure 4 and Table 2 that when the viscosity coefficient of the eddy current damper increases from 0 Ns/m to 236 Ns/m and the measured value of the equivalent damping ratio of the model structure increases from 0.67% to 2.29%, the resulting additional damping ratio increased from 0 to 1.62%. According to the analysis of equation (15), the analytical solution of the additional damping ratio of the structure produced by the damper increases from 0 to 1.59%. The analytical solution of the additional damping ratio of the structure is consistent with the test results, which verifies the analytical solution's accuracy.

5. Wind-Induced Vibration Response

High-pier cantilever construction of bridges and wind turbine towers are prone to vortex-induced resonance and buffeting under the action of fluctuating wind under wind loads. Taking the test model as the research object, ignoring the influence of friction, the damping cable's influence on the structure vortex-induced resonance and random wind load is simulated.

In this section, we consider the force vibration of the control system, added an external excitation F is applied to the top of the model structure; then, the motion equation can be obtained as

$$m_\rho \ddot{Z}(t)\int_0^H \phi^2(x)\mathrm{d}x + M\ddot{Z}(t)\phi^2(x_A) + EIZ(t)\int_0^H \left(\frac{\mathrm{d}^2\phi(x)}{\mathrm{d}x^2}\right)^2 \mathrm{d}x + k_2\left(\phi(x_B)Z(t)\cos\theta - y\right)\phi(x_B)\cos\theta + c\left(\dot{Z}(t)\phi(x_B)\cos\theta - \dot{y}\right)\phi(x_B)\cos\theta = F\phi^2(x_A), \tag{21a}$$

$$m_d\ddot{y} - k_2\left(\phi(x_B)Z(t)\cos\theta - y\right) + k_3 y = c\left(\dot{Z}(t)\phi(x_B)\cos\theta - \dot{y}\right). \tag{21b}$$

5.1. Vortex-Induced Resonance Response. In this subsection, we discuss the damping effect of the damping cable; then, the vortex-induced force can be approximately expressed as $F = F_0 \sin \omega_d t$, so as to compare and analyze the damping effect of different parameters of the damping cable on the structure under the simple harmonic excitation, where the vortex excitation force amplitude $F_0 = 10$ N. Using the method of step-by-step integral, the relationship between the vibration displacement time history of the top of the structure and the different viscous coefficients of the dampers under simple harmonic loads is shown in Figure 5. It can be seen from the figure that when the structure undergoes vortex-induced resonance, the structural amplitude gradually increases and finally enters a steady-state vibration state. Under the action of a small vortex excitation force, a low damping tower structure will also vibrate greatly.

As shown in Figure 6, the root mean square of the vibration displacement at the top of the structure decreases as

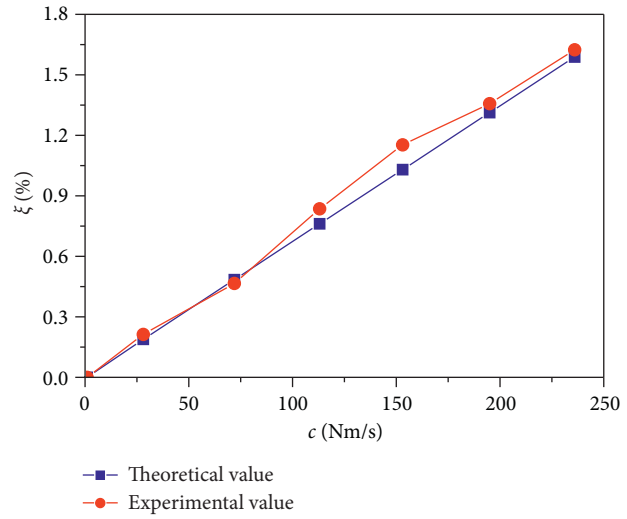

Figure 4: Additional damping ratio of experimental value and theoretical value.

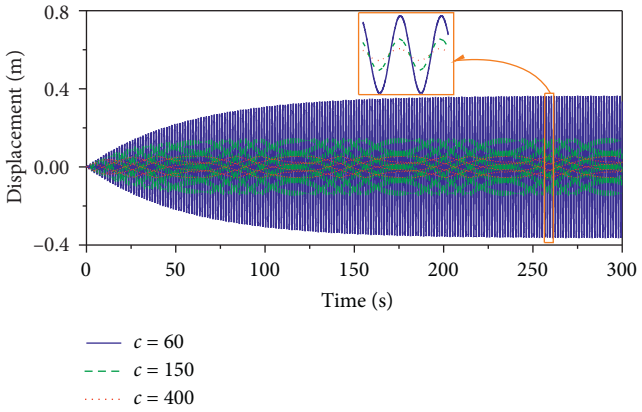

Figure 5: Structural response displacement time history under vortex excitation.

the viscosity coefficient of the damper increases. And the root mean square of the vibration displacement at the top of the structure decreases as the installation height h/H of the damping cable increases, as shown in Figure 7. Therefore, increasing the installation height h of the damping cable as much as possible and increasing the viscosity coefficient c of the damper can well suppress the amplitude of the vortex-induced resonance of a high-rise structure.

5.2. Dynamic Response with Pulsating Wind Excitation. The wind load time history is calculated based on the measured wind speed as shown in Figure 8. The wind speed data comes from the actual measurement of a 130 m high tower top of a cable-stayed bridge, and the sampling frequency is 32 Hz, which can accurately reflect the random characteristics of the wind load. The average value is subtracted from the wind load to obtain the wind load buffeting force loading $F(t)$, and the wind load pulsed power spectrum is shown in Figure 9. The figure shows that the random wind load pulsation force contains multiple frequency

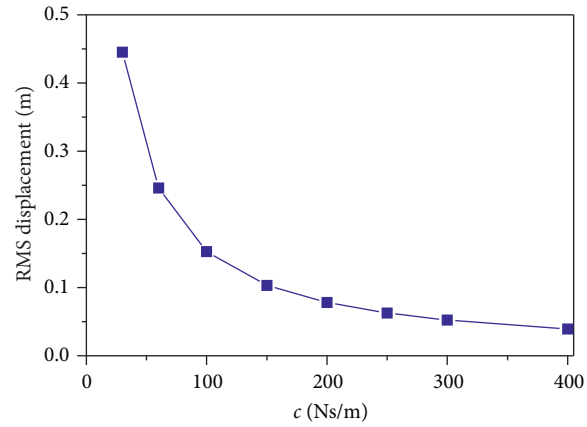

Figure 6: The relationship between the root mean square of structural displacement response and the viscosity coefficient of damper.

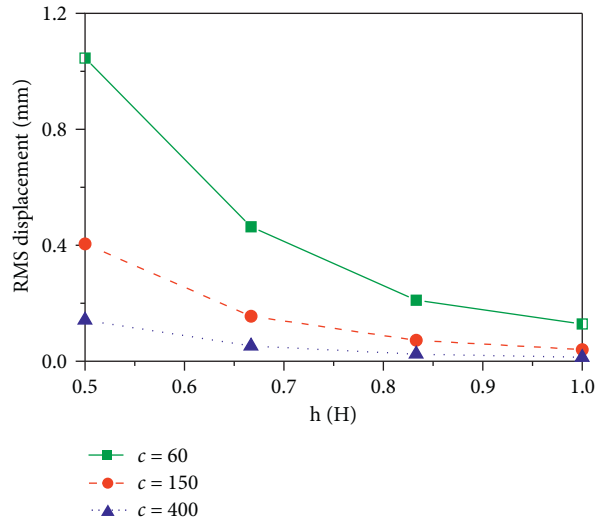

Figure 7: The relationship between the root mean square of structural displacement response and the installation height of damping cable h/H.

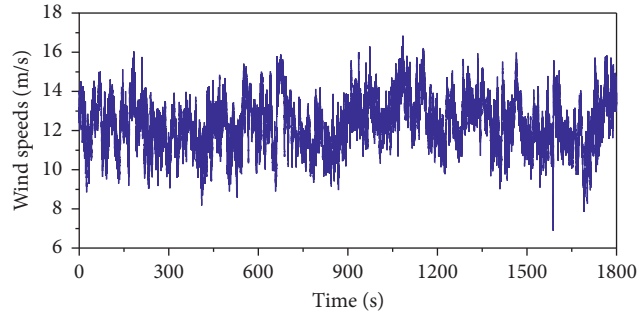

Figure 8: Wind speed time history curve.

components. The damping cable installation height h and the damper viscosity coefficient c are used to analyze the suppression effect of the damping cable on the structure buffeting, and the pulsating force $F(t)$ is substituted into equation (18) to calculate the structural dynamic response.

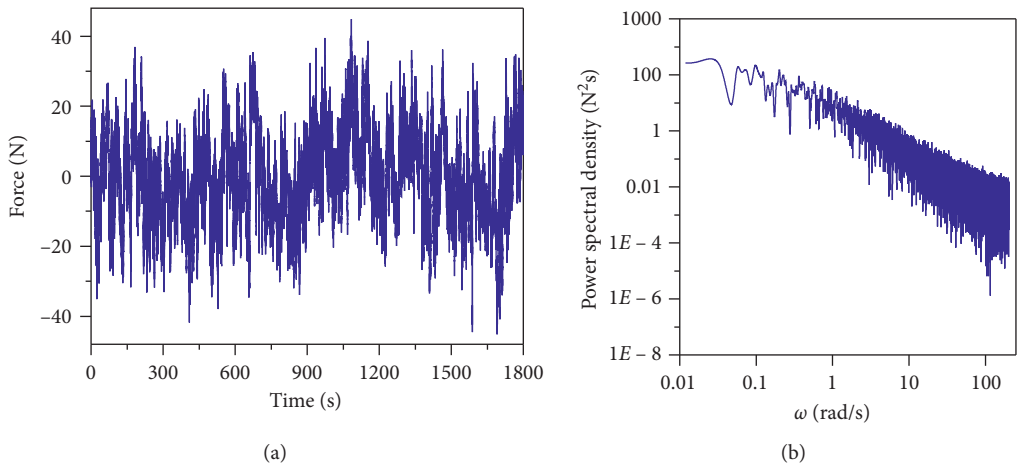

Figure 9: Buffeting force loading curve and pulse power spectrum.

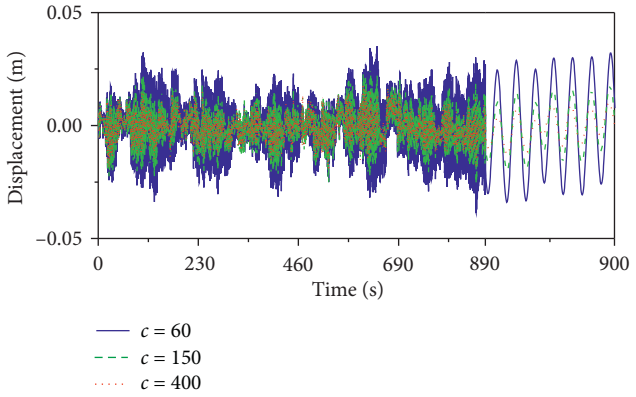

Figure 10: Structural response displacement time history under pulsating wind.

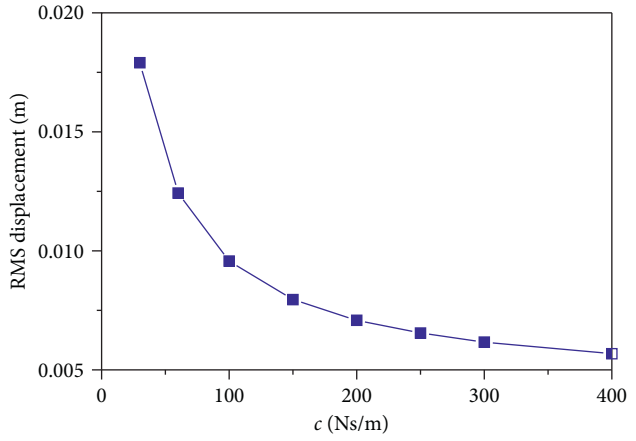

Figure 11: The relationship between the root mean square of structural displacement response and the viscosity coefficient of damper.

Then, the relationship between the vibration displacement time history of the top of the structure and the different viscosity coefficients of the damper under the action of pulsating wind load is shown in Figure 10. The structure has obvious buffeting under the action of the pulsating force.

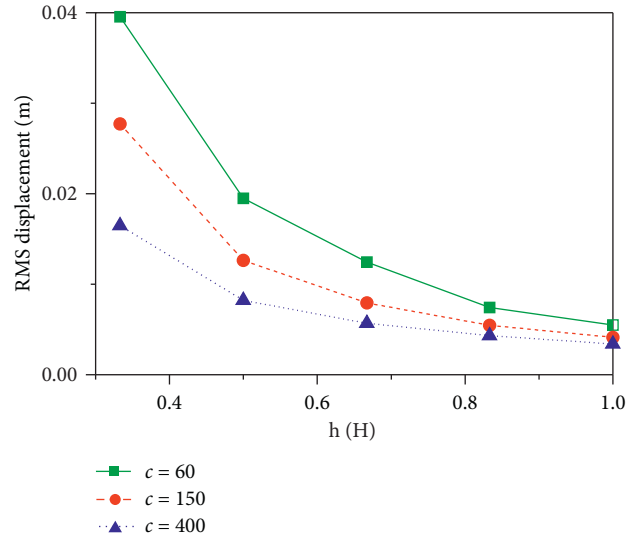

Figure 12: The relationship between the root mean square of structural displacement response and the installation height of damping cable h/H.

The calculation results show that as the viscosity coefficient of the damper increases, the structural amplitude decreases, and the relationship between the root mean square displacement and the viscosity coefficient of the damper is shown in Figure 11. The root mean square of the vibration displacement at the top of the structure also decreases as the installation height h/H of the damping cable increases, as shown in Figure 12.

6. Conclusions

In this study, the wind-induced vibration control of high-rise structures via compound damping cable has been investigated. First, the Lagrange's equation was applied to derive the motion equation of the vibration control system, and the vibration reduction mechanism of compound damping cables is introduced. Then, the characteristic problem has been determined. Following, the experimental

and theoretical results are applied to investigate the structural response under wind load.

The vibration displacement time history of the top of the structure under the action of simple harmonic vortex excitation is obtained. The structure is under the action of random fluctuating wind load, the top vibration displacement time history and acceleration time history. The relationship between the structural vibration displacement root means square, acceleration root mean square, and the different viscosity coefficients of the dampers in the composite damping cable and the different installation heights of the damping cables are studied. The analysis results show that for low damping and high-rise structure, a small vortex-induced force will cause the structure to vibrate greatly. The damping cable can greatly reduce the amplitude of the vortex-induced resonance of the structure. The root means square of the structural vibration displacement varies with the viscosity coefficient and damping of the damper. The installation height of the main cable is greatly reduced. Structure buffeting occurs under the action of wind load pulse force, and the root means square of structural vibration displacement and root mean square of acceleration both decrease rapidly with the increase of the viscosity coefficient of the damper and the installation height of the main cable of the damping cable.

Data Availability

No data were used to support the findings of this study.

Conflicts of Interest

The authors declare that they have no conflicts of interest.

Authors' Contributions

All authors actively contributed to the study. J.Yu. conceived the idea of this research and wrote the article, Z.B and X.Q. implemented the various mathematical expressions and experimental analyzed, and J.P. revised the article.

Acknowledgments

The study was supported by the National Natural Science Foundation of China (51778228 and 11402085) and Scientific Research Fund of Hunan Provincial Education (19B192).

References

[1] Q. Yang, R. Ma, and X. H. Hu, "Study of pier system of high-rise pier continuous rigid frame bridge based on wind resistance performance," *Journal of Highway and Transportation Research and Development*, vol. 33, no. 3, pp. 76–81, 2016.

[2] J. W. Zhang, "The wind-induced response of high-pier long-span continuous rigid frame bridge," *Advanced Materials Research*, vol. 639–640, pp. 502–509, 2013.

[3] J. M. Jonkman and D. Matha, "Dynamics of offshore floating wind turbines-analysis of three concepts," *Wind Energy*, vol. 14, no. 4, pp. 557–569, 2011.

[4] L. Chen, B. Basu, and S. R. K. Nielsen, "A coupled finite difference mooring dynamics model for floating offshore wind turbine analysis," *Ocean Engineering*, vol. 162, pp. 304–315, 2018.

[5] S. Sarkar and A. Chakraborty, "Development of semi-active vibration control strategy for horizontal axis wind turbine tower using multiple magneto-rheological tuned liquid column dampers," *Journal of Sound and Vibration*, vol. 457, pp. 15–36, 2019.

[6] R. C. Battista, R. S. Rodrigues, and M. S. Pfeil, "Dynamic behavior and stability of transmission line towers under wind forces," *Journal of Wind Engineering & Industrial Aerodynamics*, vol. 91, no. 8, pp. 1051–1067, 2003.

[7] P. Zhang, G. B. Song, H. N. Li, and Y. X. Lin, "Seismic control of power transmission tower using pounding TMD," *Journal of Engineering Mechanics*, vol. 139, no. 10, pp. 1395–1406, 2013.

[8] P. J. Carrato and K. Santamont, "Tuned mass damper control of cross-wind excitation of a solar tower," *Structures Congress*, vol. 1, pp. 1463–1472, 2012.

[9] P. Xiang and A. Nishitani, "Seismic vibration control of building structures with multiple tuned mass damper floors integrated," *Earthquake Engineering & Structural Dynamics*, vol. 43, no. 6, pp. 909–925, 2014.

[10] J. Peng, M. J. Xiang, L. H. Wang, X. Z. Xie, H. X. Sun, and J. D. Yu, "Nonlinear primary resonance in vibration control of cable-stayed beam with time delay feedback," *Mechanical Systems and Signal Processing*, vol. 137, Article ID 106488, 2020.

[11] Y. Zhou, D. Y. Wang, and X. X. Deng, "Optimum study on wind-induced vibration control of high-rise buildings with viscous dampers," *Wind and Structures, An International Journal*, vol. 11, no. 6, pp. 497–512, 2008.

[12] S. Y. Li, M. Liu, H. X. Li, Y. Hui, and Z. Q. Chen, "Effects of structural damping on wind-induced responses of a 243-meter-high solar tower based on a novel elastic test model," *Journal of Wind Engineering & Industrial Aerodynamics*, vol. 172, pp. 1–11, 2018.

[13] M. Liu, S. Y. Li, and Z. Q. Chen, "Mitigation of wind-induced responses of cylinder solar tower by a tiny eddy current tuned mass damper based on elastic wind tunnel tests," *Smart Structures and Systems*, vol. 26, no. 5, pp. 619–629, 2020.

[14] Q. Wang, H. Qiao, D. De Domenico, Z. Zhu, and Z. Xie, "Wind-induced response control of high-rise buildings using inerter-based vibration absorbers," *Applied Sciences*, vol. 9, p. 5045, 2019.

[15] Q. H. Wang, H. R. Tian, H. S. Qiao, N. D. Tiwari, and Q. Wang, "Wind-induced vibration control and parametric optimization of connected high-rise buildings with tuned liquid-column-damper–inerter," *Engineering Structures*, vol. 226, Article ID 111352, 2021.

[16] J. D. Yu, Y. R. Tang, S. F. Zhu, P. Y. Yu, and X. Y. Wang, "Compound damping cables," Chinese patent No. 201410694766, 2016.

[17] A. S. Nazmy and A. M. Abdel-Ghaffar, "Non-linear earthquake-response analysis of longspan cable-stayed bridges: theory," *Earthquake Engineering & Structural Dynamics*, vol. 19, no. 1, pp. 45–62, 1990.